

Tight-binding study of the magneto-optical properties of gapped graphene

Jesper Goor Pedersen and Thomas Garm Pedersen

Department of Physics and Nanotechnology Aalborg University, Skjernvej 4A DK-9220 Aalborg East, Denmark

(Dated: July 4, 2011)

We study the optical properties of gapped graphene in presence of a magnetic field. We consider a model based on the Dirac equation, with a gap introduced via a mass term, for which analytical expressions for the diagonal and Hall optical conductivities can be derived. We discuss the effect of the mass term on electron-hole symmetry and π - π^* symmetry and its implications for the optical Hall conductivity. We compare these results with those obtained using a tight-binding model, in which the mass is modeled via a staggered potential and a magnetic field is included via a Peierls substitution. Considering antidot lattices as the source of the mass term, we focus on the limit where the mass term dominates the cyclotron energy. We find that a large gap quenches the effect of the magnetic field. The role of overlap between neighboring π orbitals is investigated, and we find that the overlap has pronounced consequences for the optical Hall conductivity that are missed in the Dirac model.

PACS numbers: 78.20.Ls, 78.67.Wj

I. INTRODUCTION

While already the subject of a Nobel Prize in physics, research in graphene,^{1,2} a single two-dimensional sheet of carbon first isolated in 2004,³ seems to show no signs of slowing down. Initial studies have focused on the unique electronic properties of *pristine* graphene,⁴ such as, e.g., its extreme electron mobility,⁵ and a remarkably large cyclotron gap, which has led to integral quantum Hall measurements at room temperature.⁶ This feature of graphene arises due to its linear band structure near the Fermi energy, which leads to an unconventional half-integer quantum Hall effect due to the existence of a Landau level at zero energy.^{7–10} The field has recently matured to a point where a large part of the focus has shifted to the possible applications of graphene, in fields as diverse as transistors,¹¹ solar cells,¹² hydrogen storage,¹³ and touchscreen devices.¹⁴ This inevitably draws light to one of the serious drawbacks of graphene, namely its semi-metallic nature. Several ways of opening a gap in graphene have been put forth. If graphene is cut in narrow ribbons, so-called graphene nanoribbons, quantum confinement effects will induce a band gap, the size of which depends on the width of the ribbon as well as the intricacies of the ribbon edges.^{15–17} Adsorption on graphene of hydrogen has proven to be a very efficient way of inducing substantial band gaps in graphene, with fully hydrogenated graphene, termed graphane, exhibiting a band gap of several electron volts.^{18,19} We have previously suggested another means of rendering graphene semiconducting, by creating a periodic array of antidots, termed graphene antidot lattices.^{20,21} The source of the antidots may be actual perforations of the graphene sheet as envisioned in the original proposal, or it may be, e.g., patterned hydrogen adsorption.²² Transistors based on graphene antidot lattice have successfully been fabricated and characterized.^{23,24}

Irrespective of the specific mechanism responsible for the band gap, the simplest and most general way of

modeling it is through a mass term. Carriers near the Fermi level of graphene can be described via a Hamiltonian that resembles the Dirac Hamiltonian of massless neutrinos,²⁵ which has led to the term massless Dirac fermions being applied to the low-energy excitations of pristine graphene. Adding a term that acts oppositely on each sublattice is equivalent to adding a mass to these otherwise massless quasiparticles and consequently induces a band gap of twice the magnitude of the mass term. This results in so-called *gapped graphene*.

While the focus of much research is now on inducing a band gap in graphene, the field remains at a point where the fundamental properties of the gapped structures remain to be investigated. With this in mind, we focus in this paper on investigating the magneto-optical properties of gapped graphene. Previous studies of such properties have considered excitonic effects as the source of the mass term,^{26,27} we have in mind structures such as graphene antidot lattices, for which substantial band gaps can be induced. Focus will thus largely be on the limit in which the mass term dominates or is comparable to the cyclotron energy. While the Dirac equation provides a reasonable approximation of the low-energy structure of graphene, we extend previous studies of magneto-optical properties by comparing with results of tight-binding models. Of particular interest is the effect of including the overlap between neighboring π orbitals, which is of the order $s = 0.1$ and thus hardly insignificant. It is well-known that the overlap breaks electron-hole symmetry in the spectrum of graphene,⁴ which is of significant consequence for the magneto-optical properties of gapped graphene. In particular, we demonstrate that the broken symmetry results in a much richer structure of the optical Hall conductivity of gapped graphene. Also, a non-zero optical Hall conductivity is found, even for a chemical potential sitting in the middle of the gap, where the electron-hole symmetry inherent in the other models dictates a vanishing optical Hall conductivity.

The article is organized as follows. In section II we

first present the Dirac model, and discuss some intriguing features of the Dirac model related to valley asymmetry before presenting analytical expressions for the optical conductivities. These expressions were first derived in a slightly different manner by Gusynin *et al.* in Ref. 27. We then present the tight-binding model, emphasizing the role of overlap between neighboring π orbitals. We generalize previous results regarding the role of overlap in pristine graphene to the case of gapped graphene. In section III we present the results of the different methods. We first focus on the diagonal optical conductivity and then move on the optical Hall conductivity. We compare the three different methods and discuss the effect of the mass term, particularly in the regime where the mass term dominates the cyclotron energy. We illustrate the particular importance of including overlap in the tight-binding model in relation to the optical Hall conductivity. Finally, in IV we summarize our findings.

II. MODELS

We consider gapped graphene, i.e. including a mass term, and include a magnetic field applied perpendicular to the graphene plane, $\mathbf{B} = B\hat{\mathbf{z}}$. We choose the Landau gauge, $\mathbf{A} = Bx\hat{\mathbf{y}}$, and assume $B > 0$ throughout the article. To calculate the optical response, we use the Kubo-Greenwood formula

$$\frac{\sigma_{\alpha\beta}(\omega)}{\sigma_0} = -i \frac{4\hbar^2}{Am^2} \times \sum_{n,m} \frac{[n(E_{\nu_n}) - n(E_{\nu_m})] \Pi_{\nu_n\nu_m}^\alpha \Pi_{\nu_m\nu_n}^\beta}{E_{\nu_m,\nu_n} [E_{\nu_m,\nu_n} - (\hbar\omega + i\hbar\Gamma)]}, \quad (1)$$

where the sum is over all states, each described by a complete set of quantum numbers, ν_n . Here, $E_{\nu_m,\nu_n} = E_{\nu_m} - E_{\nu_n}$, while $n(E)$ is the Fermi distribution function, A is the unit cell area, $\hbar\Gamma$ represents a broadening term, and we have normalized with the zero-frequency graphene conductivity $\sigma_0 = e^2/(4\hbar)$. Also, we have introduced $\Pi_{\nu_n\nu_m}^\alpha$ as the α -component of the canonical momentum matrix elements $\mathbf{\Pi}_{\nu_n\nu_m} = \langle \nu_n | \mathbf{\Pi} | \nu_m \rangle$, with $\mathbf{\Pi} = \mathbf{p} + e\mathbf{A}$. To evaluate the momentum matrix elements we will make use of the commutator relation $\mathbf{\Pi} = im\hbar^{-1}[H, \mathbf{r}]$.

In order to make the comparison with tight-binding results more clear, and to illustrate in detail some of the intriguing properties of the model, we will proceed by deriving analytical results of the optical conductivity of gapped graphene, in a model based on the Dirac equation. This will serve to highlight the differences and similarities between the Dirac and the tight-binding treatment of the problem, and provide us with some analytical expressions with which to compare the tight-binding results. We stress that the analytical expressions for the optical conductivity have already been derived previously by Gusynin *et al.* in Ref. 27, although with a slightly different approach than the one we will adopt. We thus

repeat some of these results as well as others by Jiang *et al.*²⁸, in order to assist in the comparison with the tight-binding results later. Also, the derivation will serve to clarify the effect of the mass term on the symmetry between electron and hole states, which has significant implications for the optical Hall conductivity.

A. Dirac equation

The low-energy excitations of graphene near the K valley are well described by a Dirac Hamiltonian²⁵ $H_K = v_F \mathbf{\Pi} \cdot \boldsymbol{\sigma} + \Delta\sigma_z$, with $\boldsymbol{\sigma} = (\sigma_x, \sigma_y)$ where σ_i are Pauli spin matrices. Here, we have included a mass term $\Delta\sigma_z$, which breaks the sublattice symmetry and adds a band gap to graphene of size 2Δ . The two inequivalent valleys of graphene are related via time-reversal symmetry and a Hamiltonian valid near the K' valley is thus obtained by substituting $\boldsymbol{\sigma} \rightarrow \boldsymbol{\sigma}^*$. In matrix notation, the Hamiltonian thus reads

$$H = \begin{bmatrix} \Delta & \Pi_\mp \\ \Pi_\pm & -\Delta \end{bmatrix}. \quad (2)$$

Here, the upper (lower) sign corresponds to the K (K') valley, and we have introduced $\Pi_\pm = v_F(p_x \pm ip_y \pm ieBx)$, with v_F the Fermi velocity of graphene. The eigenvalues of this Hamiltonian are²⁸

$$\begin{aligned} E_n^K &= \text{sgn}(n) \sqrt{\Delta^2 + \hbar^2 \omega_c^2 |n|} - \delta_{n0} \Delta, \quad n = 0, \pm 1, \dots \\ E_n^{K'} &= \text{sgn}(n) \sqrt{\Delta^2 + \hbar^2 \omega_c^2 |n|} + \delta_{n0} \Delta, \quad n = 0, \pm 1, \dots \end{aligned} \quad (3)$$

where $\omega_c = \sqrt{2}v_F/l_B$, with the magnetic length $l_B = \sqrt{\hbar/(eB)}$, and we define $\text{sgn}(0) = 0$. This results suggest that in the presence of a mass term, particle-hole symmetry is no longer retained in each individual valley, where it is broken by the single $E_0 = \pm\Delta$ eigenstate.²⁸ In addition to the absence of particle-hole symmetry in the energy spectrum, we find that the general $\pi-\pi^*$ symmetry between electron-hole pairs of eigenstates is broken, because the mass term breaks sublattice symmetry. Letting A_{nk}^κ and B_{nk}^κ denote the individual spinor components of the eigenstates, we find that while in the absence of a mass term, the $\pi-\pi^*$ symmetry relates a given hole state to its corresponding electron state via $\Psi_{-n,k}^K = (-A_{nk}^K, B_{nk}^K)^T$, the mass term results in a relation instead between states in opposite valleys, $\Psi_{-n,k}^K = (B_{nk}^{K'}, A_{nk}^{K'})^T$. We will see that this has particular consequences for the optical Hall conductivity in gapped graphene.

To evaluate the momentum matrix elements we note that the commutator relation yields $\mathbf{\Pi}^K = mv_F \boldsymbol{\sigma}$ while $\mathbf{\Pi}^{K'} = (\mathbf{\Pi}^K)^*$. This yields the transition rule $|m\rangle = |n| \pm 1$ for optical transitions $|n\rangle \rightarrow |m\rangle$. We find that the optical conductivity tensor can then be written in the

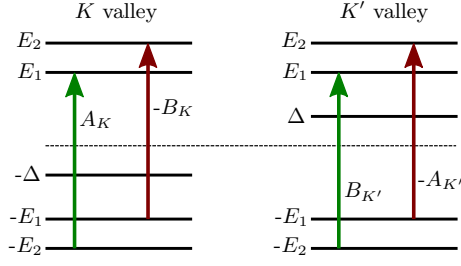


FIG. 1: (Color online) Transitions contributing to the optical Hall conductivity in gapped graphene, in the case of zero temperature and chemical potential. The weights of each transition is indicated, with color indicating the sign. Note that for vanishing gap, $A_\kappa = B_\kappa$ and the Hall conductivity vanishes within each valley. This does not hold in the gapped case, where instead contributions from opposite valleys cancel.

form

$$\begin{aligned} \frac{\sigma_{x\beta}(\Omega)}{\sigma_0} &= (-i)^{\delta_{\beta,x}} 3\phi \\ &\times \sum_{n,m} [\delta_{|n|-1,|m|} (A_K(n,m) + B_{K'}(n,m)) \\ &+ (-1)^{\delta_{\beta,y}} \delta_{|n|,|m|-1} (B_K(n,m) + A_{K'}(n,m))] \end{aligned} \quad (4)$$

where all energies are now in units of the hopping element t , $\Omega = \hbar\omega/|t|$ and $\gamma = \hbar\Gamma/|t|$, and we have introduced the relative magnetic flux $\phi = Ba^2/\Phi_0$, with the magnetic flux quantum $\Phi_0 = \pi\hbar/e$. Also, we define

$$\begin{aligned} A_\kappa(n,m) &= \frac{[n(\epsilon_n^\kappa) - n(\epsilon_m^\kappa)] |a_n^\kappa|^2 |b_m^\kappa|^2}{(\epsilon_m^\kappa - \epsilon_n^\kappa) [(\epsilon_m^\kappa - \epsilon_n^\kappa) - (\Omega + i\gamma)]}, \\ B_\kappa(n,m) &= \frac{[n(\epsilon_n^\kappa) - n(\epsilon_m^\kappa)] |b_n^\kappa|^2 |a_m^\kappa|^2}{(\epsilon_m^\kappa - \epsilon_n^\kappa) [(\epsilon_m^\kappa - \epsilon_n^\kappa) - (\Omega + i\gamma)]}, \end{aligned} \quad (5)$$

where $\epsilon_n^\kappa = E_n^\kappa/|t|$, with $\kappa \in \{K, K'\}$. Also, we have introduced $a_n^\kappa = \text{sgn}(E_n^\kappa + \Delta) \sqrt{(1 + \Delta/E_n^\kappa)/2}$ and $b_n^\kappa = i\sqrt{(1 - \Delta/E_n^\kappa)/2}$. In terms of the relative magnetic flux $\epsilon_n^\kappa = \text{sgn}(n) \sqrt{\delta^2 + (3\pi/2)\phi|n|} \mp \delta_{n0}\delta$. Note that the expressions in Eq. (5) only differ for the different valleys if the $n = 0$ state is involved in the transition.

The expression Eq. (4) for the optical conductivity highlights an interesting feature of gapped graphene. Ordinarily, at zero temperature and chemical potential, $\pi - \pi^*$ symmetry means that contributions from transitions $|-n\rangle \rightarrow |m\rangle$ and $|-m\rangle \rightarrow |n\rangle$ exactly cancel in the sum for the off-diagonal optical conductivity.³⁰ Letting $\Delta = 0$ we indeed find $|a_n|^2 = |b_n|^2$ and thus an exact cancellation of terms in the sum in Eq. (4), even if restricted to just a single valley. However, for $\Delta \neq 0$ this equality no longer holds and the lack of $\pi - \pi^*$ symmetry results in a non-zero optical Hall conductivity within each individual valley, as discussed also in the DC case by Jiang *et al.*²⁸ Instead, the modified symmetry induced by the mass term between electron and hole states in *opposite* valleys means that contributions from transitions $|-n\rangle \rightarrow |m\rangle$ in one valley are canceled by transitions $|-m\rangle \rightarrow |n\rangle$ in the opposite valley, resulting in the expected $\sigma_{xy}(\omega) = 0$ at zero temperature and chemical potential, as illustrated in Fig. 1. It is thus crucial to take into account both valleys, and to treat the asymmetry of the valleys with respect to energy spectrum and eigenstates properly.

In the general case, summing contributions from both valleys, the diagonal optical conductivity can be written

$$\begin{aligned} \frac{\sigma_{xx}(\omega)}{\sigma_0} &= -i3(\Omega + i\gamma)\phi \times \sum_{n=0}^{\infty} \left[\left(1 - \frac{\delta^2}{\epsilon_n \epsilon_{n+1}}\right) \times \frac{[n(-\epsilon_{n+1}) - n(-\epsilon_n)] + [n(\epsilon_n) - n(\epsilon_{n+1})]}{(\epsilon_{n+1} - \epsilon_n) [(\epsilon_{n+1} - \epsilon_n)^2 - (\Omega + i\gamma)^2]} \right. \\ &\quad \left. + \left(1 + \frac{\delta^2}{\epsilon_n \epsilon_{n+1}}\right) \times \frac{[n(-\epsilon_{n+1}) - n(\epsilon_n)] + [n(-\epsilon_n) - n(\epsilon_{n+1})]}{(\epsilon_{n+1} + \epsilon_n) [(\epsilon_{n+1} + \epsilon_n)^2 - (\Omega + i\gamma)^2]} \right], \end{aligned} \quad (6)$$

while the optical Hall conductivity reads

$$\begin{aligned} \frac{\sigma_{xy}(\omega)}{\sigma_0} &= 3\phi \sum_{n=0}^{\infty} ([n(-\epsilon_{n+1}) - n(-\epsilon_n)] - [n(\epsilon_n) - n(\epsilon_{n+1})]) \\ &\times \left[\left(1 - \frac{\delta^2}{\epsilon_n \epsilon_{n+1}}\right) \frac{1}{(\epsilon_{n+1} - \epsilon_n)^2 - (\Omega + i\gamma)^2} + \left(1 + \frac{\delta^2}{\epsilon_n \epsilon_{n+1}}\right) \frac{1}{(\epsilon_{n+1} + \epsilon_n)^2 - (\Omega + i\gamma)^2} \right], \end{aligned} \quad (7)$$

where $\delta = \Delta/t$ and we have defined $\epsilon_0 = \delta$. These results

are in agreement with those of Gusynin *et al.* in Ref. 27,

while derived in a different manner. We state them again here for completeness.

B. Tight-binding

Graphene is relatively well described in a nearest-neighbor tight-binding (TB) framework, considering only π -electrons. While commonly π -orbitals $\varphi(\mathbf{r} - \mathbf{R})$ centered on different sites \mathbf{R} are assumed orthogonal, we will consider also the case where the overlap between neighboring orbitals is included via the overlap integral $s = 0.1$. This turns out to have a significant impact on the off-diagonal term of the optical conductivity tensor. To include the effects of a magnetic field, we use the Peierls substitution, i.e. we adopt a minimum coupling substitution $\mathbf{p} \rightarrow \mathbf{p} + e\mathbf{A}$ and choose the basis set $\langle \mathbf{r} | \mathbf{R} \rangle = e^{i\phi(\mathbf{R}, \mathbf{r})} \varphi(\mathbf{r} - \mathbf{R})$, where the phase factor is given as a line integral³¹

$$\phi(\mathbf{R}, \mathbf{r}) = \frac{e}{\hbar} \int_{\mathbf{R}}^{\mathbf{r}} \mathbf{A} \cdot d\mathbf{l}. \quad (8)$$

In this basis, the Hamiltonian matrix elements can then be approximated as

$$\langle \mathbf{R} | H | \mathbf{R}' \rangle = \langle \mathbf{R} | H_0 | \mathbf{R}' \rangle e^{i\phi(\mathbf{R}, \mathbf{R}')}, \quad (9)$$

where H_0 denotes the Hamiltonian in absence of a magnetic field. In a coordinate system where the x axis is aligned with carbon bonds, see Fig. 2, the phase factor becomes

$$\phi(\mathbf{R}, \mathbf{R}') = \frac{\pi}{2} \frac{B}{\Phi_0} (x + x') (y' - y). \quad (10)$$

Because of the $(x + x')$ term, we are forced to choose a unit cell substantially larger than the Wigner–Seitz cell of graphene in order to retain periodicity in the problem. In particular, we use a rectangular unit cell of area $L_x \times L_y$, with $L_x = 4\Phi_0/(Ba)$ and $L_y = a$, where $a = 2.46 \text{ \AA}$ is the graphene lattice constant. The unit cell is illustrated in Fig. 2. Letting N denote the number of atoms in the magnetic unit cell, we have $N = 16\Phi_0/(\sqrt{3}a^2) \times B^{-1} \simeq 316 \cdot 10^3 \text{ T} \times B^{-1}$, illustrating the disadvantage of the tight-binding approach, namely that very large unit cells are required in order to simulate realistically small magnetic field strengths.

Analogously to the case of the Dirac equation, a gap can be introduced in the tight-binding description by adding a staggered potential with opposite sign on each sublattice, i.e. taking diagonal elements $\langle \mathbf{R} | H | \mathbf{R} \rangle = \epsilon_\pi + (-1)^n \Delta$, with $n = 0, 1$ for orbitals sitting on the A and B sublattice, respectively. Here, for generality, we have included the on-site energy ϵ_π of the π -orbitals.

If we take into account the overlap between neighboring π -orbitals, the problem becomes that of a generalized eigenvalue problem. However, advantage can be taken of the similar form of the Hamiltonian $\hat{\mathbf{H}}$ and the overlap

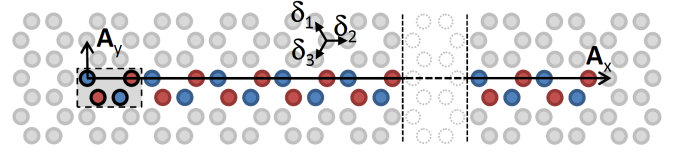


FIG. 2: (Color online) Unit cell used in the tight-binding calculations. The colored circles indicate the carbon atoms included in the unit cell, with red and blue indicating different sublattices. The dashed rectangle indicates the fundamental unit cell, which is repeated in order to ensure translational symmetry. The lattice vectors of the enlarged unit cell are denoted $\mathbf{A}_x = L_x \hat{x}$ and $\mathbf{A}_y = L_y \hat{y}$. Also shown are the three nearest neighbor vectors δ_n .

matrix $\hat{\mathbf{S}}$ in the chosen basis if we consider just nearest-neighbor coupling terms. In particular, the generalized eigenvalue problem can be written in the form

$$\begin{bmatrix} (\epsilon_\pi + \Delta) \hat{\mathbf{I}} & t \hat{\mathbf{F}} \\ t \hat{\mathbf{F}}^\dagger & (\epsilon_\pi - \Delta) \hat{\mathbf{I}} \end{bmatrix} \begin{bmatrix} \mathbf{v}_A \\ \mathbf{v}_B \end{bmatrix} = E \begin{bmatrix} \hat{\mathbf{I}} & s \hat{\mathbf{F}} \\ s \hat{\mathbf{F}}^\dagger & \hat{\mathbf{I}} \end{bmatrix} \begin{bmatrix} \mathbf{v}_A \\ \mathbf{v}_B \end{bmatrix}, \quad (11)$$

where $\hat{\mathbf{I}}$ is the identity matrix, the eigenvectors have been separated into components on different sublattices, and we have introduced the nearest-neighbor transfer integral t , evaluated in the absence of a magnetic field. The similar form of the matrices allows us to rewrite the problem as an ordinary eigenvalue problem for either sublattice, and in this way arrive at an equation

$$\frac{(E - \epsilon_\pi)^2 - \Delta^2}{(Es - t)^2} = \frac{(E_0 - \epsilon_\pi)^2 - \Delta^2}{t^2}, \quad (12)$$

relating the eigenvalues E to the eigenvalues E_0 , obtained by ignoring the overlap. This is readily solved to yield the explicit relation

$$E = \frac{1}{t - s^2 (\xi_0^2 - \Delta^2)/t} \times \left\{ t\epsilon_0 - s (\xi_0^2 - \Delta^2) \pm \left[(t\epsilon_0 - s (\xi_0^2 - \Delta^2))^2 + (\xi_0^2 - \epsilon_\pi^2) (t^2 - s^2 (\xi_0^2 - \Delta^2)) \right]^{1/2} \right\}, \quad (13)$$

where $\xi_0 = E_0 - \epsilon_\pi$. Here, the sign of the square root should follow the sign of the energy E_0 . We can thus immediately determine the eigenvalues with the overlap included, without solving an additional generalized eigenvalue problem. Furthermore, we use the same eigenvectors, only properly orthonormalized according to the overlap. While using Eq. (13) to calculate the eigenvalues with overlap is exact, this way of determining the eigenvectors constitutes an approximation. However, we have confirmed numerically that this has no discernible effect of the calculated optical conductivities so long as $s\Delta \ll t$.

In addition to offering a decrease in computation time, the similarities of the $\hat{\mathbf{H}}$ and $\hat{\mathbf{S}}$ matrices allows us to

greatly simplify the calculation of the momentum matrix elements. Following ideas similar to those used by Sandu in Ref. 32 for evaluating the momentum matrix elements of ordinary graphene, we consider the Hamiltonian of the ordinary eigenvalue problem $\hat{\mathbf{H}}_S = \hat{\mathbf{S}}^{-1}\hat{\mathbf{H}}$. The inverse of the overlap matrix can be written

$$\hat{\mathbf{S}}^{-1} = \begin{bmatrix} (\hat{\mathbf{I}} - s^2 \hat{\mathbf{F}} \hat{\mathbf{F}}^\dagger)^{-1} & -s \hat{\mathbf{F}} (\hat{\mathbf{I}} - s^2 \hat{\mathbf{F}}^\dagger \hat{\mathbf{F}})^{-1} \\ -s \hat{\mathbf{F}}^\dagger (\hat{\mathbf{I}} - s^2 \hat{\mathbf{F}} \hat{\mathbf{F}}^\dagger)^{-1} & (\hat{\mathbf{I}} - s^2 \hat{\mathbf{F}}^\dagger \hat{\mathbf{F}})^{-1} \end{bmatrix}. \quad (14)$$

We now disregard terms with $s^2 \ll 1$, so that

$$\hat{\mathbf{H}}_S = \begin{bmatrix} (\epsilon_\pi + \Delta) \hat{\mathbf{I}} - st \hat{\mathbf{F}} \hat{\mathbf{F}}^\dagger & (t - s(\epsilon_\pi - \Delta)) \hat{\mathbf{F}} \\ (t - s(\epsilon_\pi + \Delta)) \hat{\mathbf{F}}^\dagger & (\epsilon_\pi - \Delta) \hat{\mathbf{I}} - st \hat{\mathbf{F}}^\dagger \hat{\mathbf{F}} \end{bmatrix}. \quad (15)$$

The form of this matrix makes it evident how the inclusion of overlap effectively results in next-nearest neighbor coupling. In the crystal momentum representation, the momentum operator is proportional to $\nabla_{\mathbf{k}} H$, which for the Hamiltonian above becomes

$$\nabla_{\mathbf{k}} \hat{\mathbf{H}}_S = \begin{bmatrix} -st \nabla_{\mathbf{k}} (\hat{\mathbf{F}} \hat{\mathbf{F}}^\dagger) & (t - s(\epsilon_\pi - \Delta)) \nabla_{\mathbf{k}} \hat{\mathbf{F}} \\ (t - s(\epsilon_\pi + \Delta)) \nabla_{\mathbf{k}} \hat{\mathbf{F}}^\dagger & -st \nabla_{\mathbf{k}} (\hat{\mathbf{F}}^\dagger \hat{\mathbf{F}}) \end{bmatrix}. \quad (16)$$

If we now assume $s\Delta \ll t$ and let $\epsilon_\pi = 0$ this matrix simplifies to

$$\nabla_{\mathbf{k}} \hat{\mathbf{H}}_S = t \begin{bmatrix} 0 & \nabla_{\mathbf{k}} \hat{\mathbf{F}} \\ \nabla_{\mathbf{k}} \hat{\mathbf{F}}^\dagger & 0 \end{bmatrix} - st \begin{bmatrix} \nabla_{\mathbf{k}} (\hat{\mathbf{F}} \hat{\mathbf{F}}^\dagger) & 0 \\ 0 & \nabla_{\mathbf{k}} (\hat{\mathbf{F}}^\dagger \hat{\mathbf{F}}) \end{bmatrix}. \quad (17)$$

For gapped graphene in the absence of a magnetic field, the second term is proportional to the unit matrix and thus does not contribute to the momentum matrix elements, meaning that the momentum operator is unaltered by the inclusion of overlap in the model, as is the case for ordinary graphene with no mass term.³² However, in the present case, where a magnetic field is included, such a simplification can no longer be made. Instead, we note that the second term relies on two small effects, that of the overlap and that of the magnetic field. Consequently, we ignore the effect of the magnetic field on the matrix elements of $\hat{\mathbf{F}}$ in this term, which allows us to disregard the second term entirely, as it no longer contributes to the momentum matrix elements. Effectively, we are thus ignoring non-orthogonality of our basis set and calculating the momentum matrix elements via $\Pi_{nm} = i(m/\hbar)H_{nm}(\mathbf{R}_m - \mathbf{R}_n)$.

In the numerical implementation of the tight-binding model we employ a simple equidistant k -point mesh. Our choice of unit cell results in negligible dispersion along k_x , so we only discretize along the k_y direction, ensuring that the folded high-symmetry points are included in the discretization. We have verified that including more than a single k_x point has no influence on the results for any realistic values of the magnetic field.

III. RESULTS AND DISCUSSION

We now turn to the results for the optical conductivity. Unless otherwise stated, from hereon we will use parameters $\epsilon_\pi = 0$, $s = 0.1$ and $t = -2.2$ eV, we include a broadening term $\hbar\Gamma = 0.05$ eV and fix the temperature at 300 K. Our choice of the value of the hopping term t is motivated by the transition energy of the saddle point resonance in ordinary graphene, which occurs at $2|t| = 4.4$ eV.^{29,30} We note that this value of the hopping term results in a Fermi velocity that does not match experimental results. Without introducing interaction terms in the form of excitonic effects, one cannot account both for the location of the saddle point resonance and the proper value of the Fermi velocity. In the end, the exact choice of hopping term does not have a qualitative influence on the results we arrive at.

Because of the inherent problems of the Peierls substitution for the tight binding method, namely the inconvenient scaling of the unit cell with magnetic field, we are limited to quite large magnetic fields. Therefore, most results will be for a substantial magnetic field of 78 T. However, we expect the qualitative features and the conclusions to be valid at more realistic magnetic fields. This claim will be substantiated when we compare the tight binding results to those obtained using the Dirac equation.

A. Diagonal conductivity

We now consider gapped graphene with a mass term $\Delta = 0.2$ eV. We fix the chemical potential at midgap, $\mu = 0$, and use $T = 300$ K. In Fig. 3 we show the resulting diagonal optical conductivity calculated using DE and TB with and without overlap. The results from all three methods indicate a very clear absorption edge, in excellent agreement with the DE solution, which predicts the first resonance peak at $\hbar\omega_0 = \Delta \left(1 + \sqrt{1 + \hbar^2 \omega_c^2 / \Delta^2}\right)$. Focusing attention on photon energies below 1.5 eV, we find almost perfect agreement between all three methods, as illustrated in the inset of Fig. 3. Here, the resonances fall perfectly on the transition energies predicted by the DE model, as indicated by the vertical lines in the inset.

However, a notable feature of the full range of energies is the peak near $2|t| = 4.4$ eV, which stems from the van Hove singularity at the M point of graphene. Naturally, such a band structure feature is not reproduced in a DE model. This M -point resonance is unaffected by the addition of a mass term, so long as $\Delta \ll t$. We note that the overlap results in a slight blueshift of the resonance peak, so that it occurs at $2|t|/(1 - s^2)$.

In Fig. 4 we show the diagonal optical conductivity in the case where the chemical potential sits on top of the lowest Landau level at $\mu = \Delta$. The DE model suggest that in this case the lowest resonance, $\hbar\omega_0$, will split into two resonances at $\hbar\omega_{\pm} = \Delta \left(\sqrt{1 + \hbar^2 \omega_c^2 / \Delta^2} \pm 1\right)$ ²⁷.

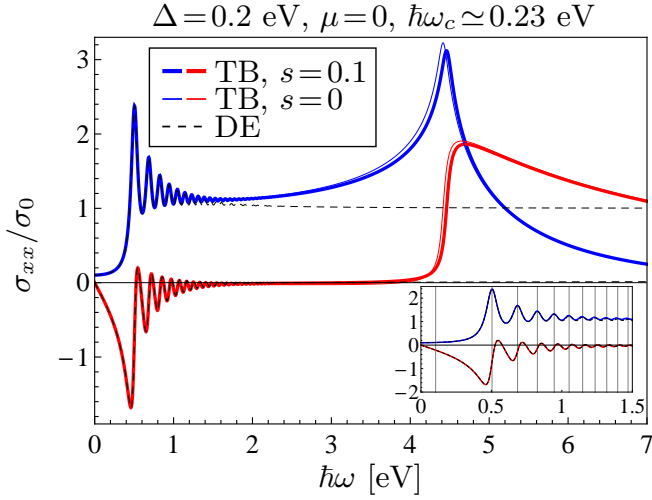


FIG. 3: (Color online) Diagonal conductivity σ_{xx} in units of the DC graphene conductivity σ_0 , as a function of photon energy $\hbar\omega$. Results are shown for a magnetic field $B = 78$ T. Thick lines indicate results from the TB model including overlap, while thin lines are without overlap. Dashed lines are DE results. Blue (red) coloring indicates the real (imaginary) part of the conductivity. Note the resonance around $\hbar\omega = 4.4$ eV, which arises due to the van Hove singularity at the M point of graphene, and is thus absent in the DE results. The inset offers a closer view of the low-energy oscillations, illustrating the excellent agreement between all three methods in this energy range. The vertical lines mark the transition energies predicted by the DE model.

Other than this splitting of the lowest resonance, the results are nearly identical to those obtained with the chemical potential at midgap. The inset in Fig. 4 again shows excellent agreement between all three methods.

In Fig. 5 we illustrate the effect of the mass term on the diagonal conductivity. We show results from the TB model with overlap, and with a value of the mass term increasing from 0.1 eV to 1 eV. We fix the chemical potential at midgap. Considering the eigenenergies obtained using the Dirac equation, $E_n = \Delta(\sqrt{1 + (\hbar^2\omega_c^2/\Delta^2)|n|} \pm 1)$, we expect that the effect of the mass term will be to compress the Landau level spacing, resulting in a nearly continuous spectrum for $\Delta \gg \hbar\omega_c$. This trend is evident in the results of Fig. 5, where we note that the oscillations due to Landau level spacing are almost completely washed out for $\Delta = 1$ eV. Also shown in the figure is the optical conductivity in the absence of a magnetic field.³³ Comparing these to the results with magnetic field, it is clear that for a sufficiently large mass term, $\Delta \gg \hbar\omega_c$, the results are nearly identical, indicating that a large mass term completely cancels the effect of the magnetic field on the diagonal optical conductivity. We stress that while the cyclotron energy in this case is so large that a mass term of the order of 1 eV is needed to counter the effect of the magnetic field, more realistic values of the magnetic field strength would of course lower this

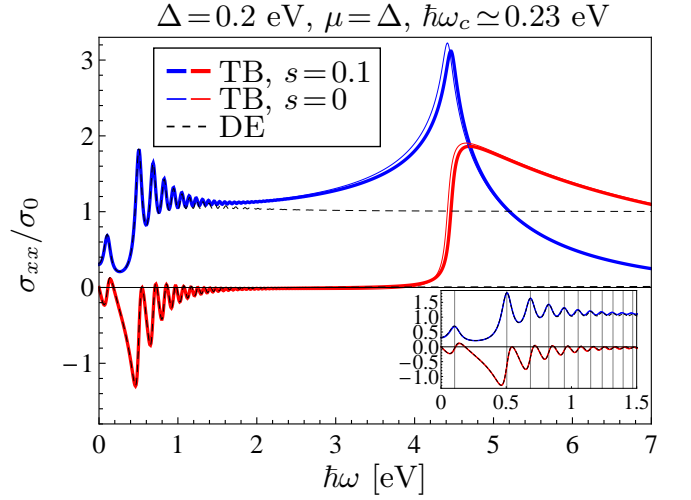


FIG. 4: (Color online) Diagonal conductivity σ_{xx} in units of the DC graphene conductivity σ_0 , as a function of photon energy $\hbar\omega$. Results are shown for a magnetic field $B = 78$ T. The chemical potential is set at the value of the mass term, $\mu = \Delta$. Thick lines indicate results from the TB model including overlap, while thin lines are without overlap. Dashed lines are DE results. Blue (red) coloring indicates the real (imaginary) part of the conductivity. The inset offers a closer view of the low-energy oscillations, illustrating the excellent agreement between all three methods in this energy range. The vertical lines mark the transition energies predicted by the DE model.

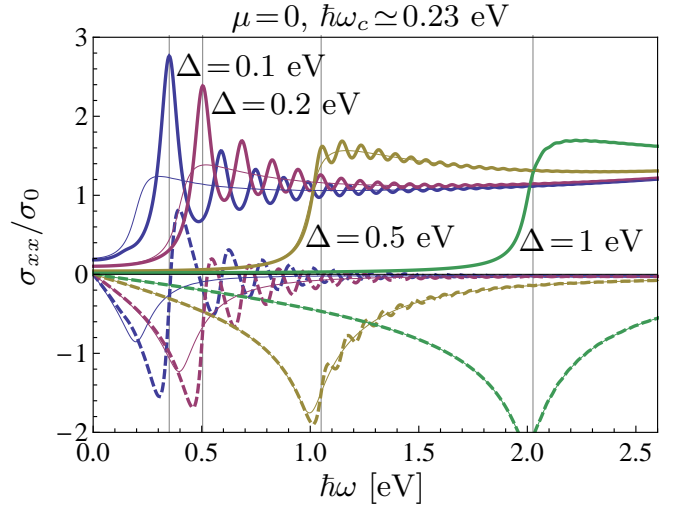


FIG. 5: (Color online) Diagonal conductivity σ_{xx} in units of the DC graphene conductivity σ_0 , as a function of photon energy $\hbar\omega$. Results are shown for a magnetic field $B = 78$ T and for four different values of the mass term, all calculated using the TB model with overlap. Full (dashed) lines indicate the real (imaginary) part of the conductivity. For comparison, the thin lines show the optical conductivity in absence of a magnetic field. The vertical lines indicate the resonance energies predicted by the DE model.

threshold significantly.

In general, we find that even at the very large magnetic field of 78 T used for these calculations, and at chemical potentials well above the value of the mass term, the results for the diagonal conductivity are in excellent agreement between the three methods, so long as photon energies are well below the M -point resonance. We see no reason why such an agreement should break down at lower field strengths, provided that broadening does not smear out the resonances, and we thus argue that the results we obtain will remain qualitatively the same also at more realistic magnetic fields, with resonances simply red-shifted in accordance with the lower cyclotron energy.

B. Hall conductivity

We now turn to the off-diagonal Hall conductivity. Before discussing the optical Hall conductivity, we focus on the DC Hall conductivity $\sigma_{xy}^0 \equiv \sigma_{xy}(0)$ as function of the chemical potential. An intriguing consequence of the linear dispersion relation of graphene is the emergence of an unconventional quantum Hall effect, with the DC Hall conductivity quantized according to $\sigma_{xy}^0 = -(4e^2/h)(n + 1/2)$, with n a positive integer or zero. This unique feature has its origin in the $n = 0$ Landau level, the degeneracy of which is half that of the higher Landau levels.^{9,34} This carries over to the case of gapped graphene, if contributions from both valleys are taken into account.²⁸

In Fig. 6 we show the DC Hall conductivity as a function of chemical potential, calculated using the three models. In these calculations, the temperature has been set to 1K and the broadening term $\hbar\Gamma$ has been omitted, in order to properly resolve the quantum Hall plateaus. In panel (a) of the figure, we show the full range of chemical potentials considered. While there is quite good agreement between all three models for low values of the chemical potential, $\mu \lesssim 0.5$ eV, the breakdown of the Dirac model is apparent at higher chemical potentials, for which the non-linear part of the band structure is probed. This results in discrepancies in the energies of the Landau levels, which is apparent in Fig. 6b. While the TB model without overlap obviously results in a slightly different Landau level structure, the values of the DC Hall conductivity still fall at the same plateaus as predicted by the DE model. The inclusion of overlap alters the results quite significantly, with any but the lowest Hall plateaus falling at non-equidistant values. We stress that these results are of course calculated for a substantial magnetic field, and we expect much better agreement between the three models when the Landau level spacing is smaller. The TB results show an abrupt change in behavior near a chemical potential of $\mu = (1 + s)|t|$, where σ_{xy}^0 suddenly changes sign. This value of the chemical potential coincides with the maximum of the band at the M point of gapped graphene without a magnetic field, as illustrated in the inset of Fig. 6. The degeneracy of the Landau

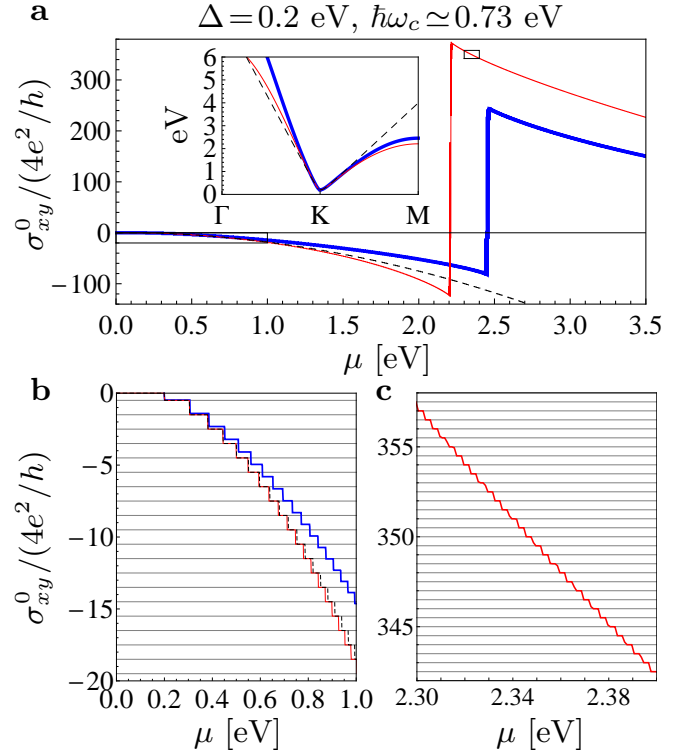


FIG. 6: (Color online) DC Hall conductivity in gapped graphene as a function of the chemical potential. The thick, blue lines are results of the TB model including overlap, while thin, red lines are without overlap. Dashed, black lines are the DE results. Note that in contrast to the other figures, here the conductivity is given in units of $4e^2/h$. (a) DC Hall conductivity in the full range of chemical potentials considered, illustrating the discrepancies between the three models and the abrupt change in behavior near $\mu = (1 + s)|t|$ for the TB model results. The inset shows the band structure of gapped graphene without magnetic field. (b) and (c) offer closer views of the regimes indicated by black rectangles in panel a. Horizontal lines in (b) indicate $\sigma_{xy}^0 = -(4e^2/h)(n + 1/2)$, while those in (c) indicate $\sigma_{xy}^0 = (2e^2/h)n$.

levels is abruptly altered at this point, with the four-fold degeneracy for Landau levels below $E = (1 + s)|t|$ changed to a two-fold degeneracy above this energy, as we have confirmed by inspection of the eigenvalues of both TB models. This results in a new structure of the quantized Hall plateaus, as shown in Fig. 6c, with the reduced degeneracy manifesting as Hall plateaus at values $\sigma_{xy}^0 = (2e^2/h)n$. As they have their origin in the non-linear part of the band structure, these features are of course entirely absent in the DE results.

We now turn to the optical Hall conductivity. As described previously and illustrated in Fig. 1, the DE model predicts an optical Hall conductivity identically zero at zero temperature and for a chemical potential fixed at midgap, due to the complete cancellation of conjugated transitions in opposite valleys. Below, we will show that this does not hold for the TB model with overlap, but for

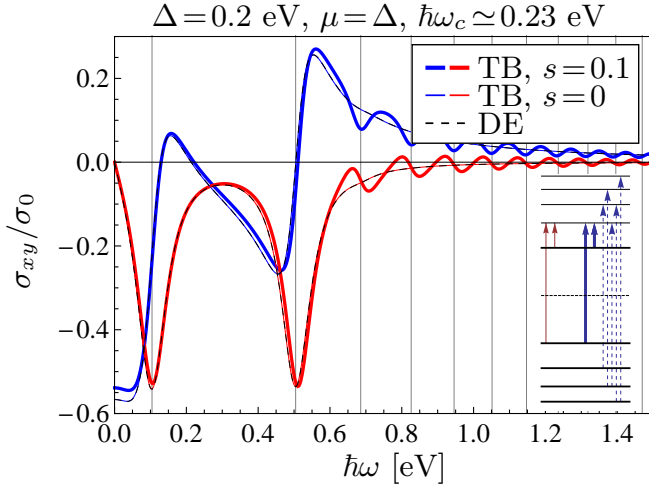


FIG. 7: (Color online) Optical Hall conductivity σ_{xy} in units of the DC graphene conductivity σ_0 , as a function of photon energy $\hbar\omega$. Results are shown for a magnetic field $B = 78$ T. The chemical potential is set at the value of the mass term, $\mu = \Delta$. Thick lines indicate results from the TB model including overlap, while thin lines are without overlap. Dashed lines are DE results. Blue (red) coloring indicates the real (imaginary) part of the conductivity. Vertical lines indicate the resonance energies predicted by the DE model. The inset illustrates the transitions contributing to the Hall conductivity. See text for more details.

now we focus on the case where the chemical potential is located at the lowest Landau level, $\mu = \Delta$. In this case, the symmetry argument obviously breaks down due to the different Fermi distribution functions of the conjugated transitions, and all three models predict non-zero Hall conductivities.

In Fig. 7 we show the optical Hall conductivity of gapped graphene with a mass term of $\Delta = 0.2$ eV and the chemical potential at $\mu = \Delta$. Common to the results of all three models are the two pronounced resonances, that the DE model predict at $\hbar\omega_{\pm} = \Delta \left(\sqrt{1 + \hbar^2 \omega_c^2 / \Delta^2} \pm 1 \right)$, similar to the lowest resonances of the corresponding diagonal conductivity shown in Fig. 4. However, contrary to the diagonal conductivity, higher-energy resonances are strongly suppressed in the case of the TB model with overlap, and are entirely absent in the two other models. This can be explained quite straightforwardly by considering the conjugate transitions and the effect of the overlap on the band structure. We illustrate this in the inset of Fig. 7. Here, the thin, red arrows indicate the transitions contributing to the optical Hall conductivity in the case of the DE model and the TB model without overlap. Because of perfect electron-hole symmetry in both these models (when including both valleys), contributions from all other transitions are canceled by their conjugates, the only transitions contributing being those involving the state at $E = \Delta$. When overlap is included (indicated by thick, blue arrows in the inset), electron-

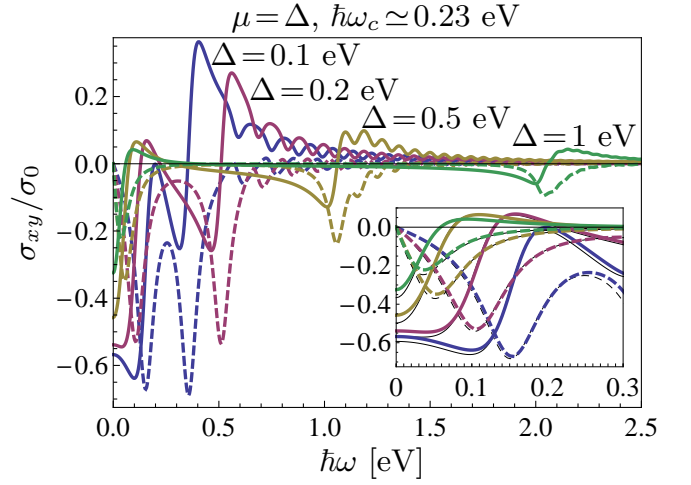


FIG. 8: (Color online) Optical Hall conductivity σ_{xy} in units of the DC graphene conductivity σ_0 , as a function of photon energy $\hbar\omega$. Results are shown for a magnetic field $B = 78$ T and for four different values of the mass term, all calculated using the TB model with overlap. The chemical potential is in each case fixed at the lowest Landau level, $\mu = \Delta$. Full (dashed) lines indicate the real (imaginary) part of the conductivity. The inset shows a closer view of the first resonance. The results of the TB model without overlap is shown by thin, black lines, illustrating the slight discrepancies between the models in this regime. The DE results are practically identical to those of the TB model without overlap.

hole symmetry is broken and the conjugate transitions no longer cancel due to a slight difference in their transition energies (dashed arrows in the inset). This results in a much richer structure of the optical Hall conductivity when including overlap, with additional resonances occurring due to transitions between higher-lying Landau levels. However, because the energy difference between electron and hole states induced by the overlap is only of the order s^2 , the strengths of these resonances are reduced significantly compared to those stemming from the $E = \Delta$ Landau level.

In Fig. 8 we illustrate the effect of the mass term on the optical Hall conductivity. We show results of the TB model with overlap, and increase the mass term from $\Delta = 0.1$ eV to $\Delta = 1$ eV, while in each case fixing the chemical potential at the energy of the lowest Landau level, $\mu = \Delta$. As for the diagonal conductivity, we clearly see that the effect of the magnetic field is strongly reduced when the mass term dominates the cyclotron energy. Thus, whereas at large values of the mass term the diagonal conductivity retains the resonance corresponding to a transition energy of roughly the size of the band gap, this resonance vanishes in the optical Hall conductivity, once the mass term grows sufficiently large. In the inset of Fig. 8, we show a closer view of the first resonance at $E_1 - \Delta$, and include results of the TB model without overlap. While there are some small discrepancies between the two models in this regime, the overall

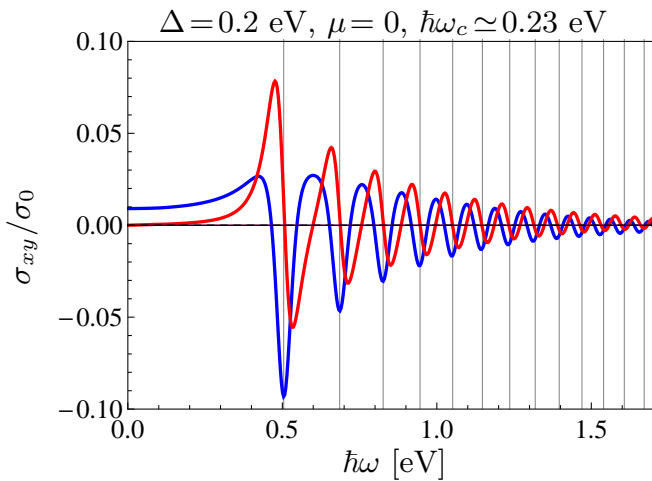


FIG. 9: (Color online) Optical Hall conductivity with a chemical potential fixed at midgap, calculated using the TB model with overlap. The vertical lines indicate the transition energies predicted by the DE model.

agreement between the models is quite good. The corresponding results of the DE model are nearly identical to those of the TB model without overlap. We note that the DC Hall conductivity is also decreased as the mass term increases, due to squeezing of the Landau level spacing.

As noted above, an interesting consequence of including overlap in the TB model is that the electron-hole symmetry is broken, and exact cancellation of conjugate transitions at zero chemical potential no longer applies. We therefore expect that the inclusion of overlap in the TB model will result in a non-zero optical Hall conductivity even at vanishing temperatures and the chemical potential fixed midgap. In Fig. 9 we illustrate this, showing the optical Hall conductivity calculated using the TB model with overlap, with a mass term $\Delta = 0.2$ eV and the chemical potential at midgap. As expected, while the other two methods predict a zero Hall conductivity, the inclusion of overlap breaks the electron-hole symmetry and results in a non-zero optical Hall conductivity. Overlap is thus a crucial ingredient for properly evaluating the optical Hall conductivity of graphene. However, we note that because it stems from the overlap, the magnitude of the Hall conductivity remains significantly lower than the case where the chemical potential sits at the lowest Landau level.

IV. SUMMARY

We have calculated the optical conductivity tensor of gapped graphene in presence of a magnetic field, by em-

ploying a Peierls substitution in a nearest-neighbor tight-binding model, both with and without overlap. By generalizing results from ordinary graphene with no magnetic field, we have found a simple relation between energy eigenvalues calculated with and without overlap, allowing us to avoid solving a large generalized eigenvalue problem to account for the overlap. This simplification is valid so long as $s\Delta \ll t$. We have compared the optical conductivities calculated using the tight-binding model with analytical expressions obtained in a Dirac equation approach.²⁷ To elucidate the differences between these two approaches we have highlighted the role played by the mass term in redefining the symmetry between electron and hole states in the Dirac model. This results in a non-zero optical Hall conductivity in individual valleys even with a chemical potential fixed in the middle of the mass gap. However, summing contributions from both valleys, the symmetry induced by the mass term between electron and hole states in opposite valleys results in an optical Hall conductivity identically zero. This result carries over to the tight-binding model without overlap, and in general we find excellent agreement between the optical Hall conductivities calculated with these two methods.

Including overlap in the tight-binding model strongly modifies this picture, because the energy spectrum no longer has perfect electron-hole symmetry. We find that this results in a much richer structure of the optical Hall conductivity, while also predicting non-zero optical Hall conductivity even with a chemical potential fixed midgap. We conclude that overlap is a crucial ingredient for a proper, full description of the off-diagonal magneto-optical properties of gapped graphene. While the optical Hall conductivity does show some significant discrepancies between the three models, in general we find that the low-energy transitions are, as expected, very well captured in the simple Dirac model. In particular, the diagonal optical conductivity at transition energies well below the saddle point resonance at 4.4 eV is almost identical between all three models.

Finally, we find that a sufficiently large mass term, much larger than the cyclotron energy, effectively washes out the influence of the magnetic field on the optical properties of gapped graphene.

Acknowledgments

Financial support from Danish Research Council FTP grant “Nanoengineered graphene devices” is gratefully acknowledged.

¹ A. K. Geim and K. S. Novoselov, Nature Materials **6**, 183 (2007).

² A. K. Geim, Science **19**, 1530 (2009).

- ³ K. S. Novoselov, A. K. Geim, S. V. Morozov, D. Jiang, Y. Zhang, S. V. Dubonos, I. V. Grigorieva, and A. A. Firsov, *Science* **306**, 666 (2004).
- ⁴ A. H. Castro Neto, F. Guinea, N. M. R. Peres, K. S. Novoselov, and A. K. Geim, *Rev. Mod. Phys.* **81**, 109 (2009).
- ⁵ S. V. Morozov, K. S. Novoselov, M. I. Katsnelson, F. Schedin, D. C. Elias, J. A. Jaszczak, and A. K. Geim, *Phys. Rev. Lett.* **100**, 016602 (2008).
- ⁶ K. S. Novoselov, Z. Jiang, Y. Zhang, S. V. Morozov, H. L. Stormer, U. Zeitler, J. C. Maan, G. S. Boebinger, P. Kim, and A. K. Geim, *Science* **315**, 1379 (2007).
- ⁷ K. S. Novoselov, A. K. Geim, S. V. Morozov, D. Jiang, M. I. Katsnelson, I. V. Grigorieva, S. V. Dubonos, and A. A. Firsov, *Nature* **438**, 197 (2005).
- ⁸ Y. Zhang, Y.-W. Tan, H. L. Stormer, and P. Kim, *Nature* **438**, 201 (2005).
- ⁹ V. P. Gusynin and S. G. Sharapov, *Phys. Rev. Lett.* **95**, 146801 (2005).
- ¹⁰ V. P. Gusynin and S. G. Sharapov, *Phys. Rev. B* **71**, 125124 (2005).
- ¹¹ Y.-M. Lin, C. Dimitrakopoulos, K. A. Jenkins, D. B. Farmer, H.-Y. Chiu, A. Grill, and P. Avouris, *Science* **327**, 662 (2010).
- ¹² H. Park, J. A. R. K. Kim, V. Bulovic, and J. Kong, *Nanotechnology* **21**, 505204 (2010).
- ¹³ S. Patchkovskii, J. S. Tse, S. N. Yurchenko, L. Zhechkov, T. Heine, and G. Seifert, *Proc. Natl. Acad. Sci. USA* **102**, 10439 (2005).
- ¹⁴ S. Bae, H. Kim, Y. Lee, X. Xu, J.-S. Park, Y. Zheng, J. Balakrishnan, T. Lei, H. Ri Kim, Y. I. Song, et al., *Nat. Nano.* **5**, 574 (2010).
- ¹⁵ K. Nakada, M. Fujita, G. Dresselhaus, and M. S. Dresselhaus, *Phys. Rev. B* **54**, 17954 (1996).
- ¹⁶ Y.-W. Son, M. L. Cohen, and S. G. Louie, *Phys. Rev. Lett.* **97**, 216803 (2006).
- ¹⁷ L. Brey and H. A. Fertig, *Phys. Rev. B* **73**, 235411 (2006).
- ¹⁸ J. O. Sofo, A. S. Chaudhari, and G. D. Barber, *Physical Review B* **75**, 153401 (2007).
- ¹⁹ D. C. Elias, R. R. Nair, T. M. G. Mohiuddin, S. V. Morozov, P. Blake, M. P. Halsall, A. C. Ferrari, D. W. Boukhvalov, M. I. Katsnelson, A. K. Geim, et al., *Science* **323**, 610 (2009).
- ²⁰ T. G. Pedersen, C. Flindt, J. Pedersen, N. A. Mortensen, A.-P. Jauho, and K. Pedersen, *Phys. Rev. Lett.* **100**, 136804 (2008).
- ²¹ T. G. Pedersen, C. Flindt, J. Pedersen, A.-P. Jauho, N. A. Mortensen, and K. Pedersen, *Phys. Rev. B* **77**, 245431 (2008).
- ²² R. Balog, B. Jrgensen, L. Nilsson, M. Andersen, E. Rienks, M. Bianchi, M. Fanetti, E. Lgsgaard, A. Baraldi, S. Lizzit, et al., *Nature Materials* **9**, 315 (2010).
- ²³ J. Bai, X. Zhong, S. Jiang, Y. Huang, and X. Duan, *Nature Nanotechnology* **5**, 190 (2010).
- ²⁴ M. Kim, N. S. Safron, E. Han, M. S. Arnold, and P. Gopalan, *Nano Lett.* **10**, 1125 (2010).
- ²⁵ G. W. Semenoff, *Phys. Rev. Lett.* **53**, 2449 (1984).
- ²⁶ V. P. Gusynin, S. G. Sharapov, and J. P. Carbotte, *Phys. Rev. Lett.* **96**, 256802 (2006).
- ²⁷ V. P. Gusynin, S. G. Sharapov, and J. P. Carbotte, *J. Phys. Cond Mat.* **19**, 026222 (2007).
- ²⁸ L. Jiang, Y. Zheng, H. Li, and H. Shen, *Nanotechnology* **21**, 145703 (2010).
- ²⁹ E. A. Taft and H. R. Phillip, *Phys. Rev.* **138**, A197 (1964).
- ³⁰ T. G. Pedersen, *Phys. Rev. B* **68**, 245104 (2003).
- ³¹ J. M. Luttinger, *Phys. Rev.* **84**, 814 (1951).
- ³² T. Sandu, *Phys. Rev. B* **72**, 125105 (2005).
- ³³ T. G. Pedersen, A.-P. Jauho, and K. Pedersen, *Phys. Rev. B* **79**, 113406 (2009).
- ³⁴ V. P. Gusynin and S. G. Sharapov, *Phys. Rev. B* **73**, 245411 (2006).
- ³⁵ D. Xiao, W. Yao, and Q. Niu, *Phys. Rev. Lett.* **99**, 236809 (2007).
- ³⁶ A. Rycerz, J. Tworzydło, and C. J. Beenakker, *Nature Physics* **3**, 172 (2007).
- ³⁷ D. Gunlycke and C.T. White, *Phys. Rev. L* **106**, 136806 (2011).